Electrochemical Control of Photoluminescence in Two-Dimensional MoS_2 Nanoflakes

Yichao Wang,[†,#] Jian Zhen Ou,[†,#,*] Sivacarendran Balendhran,[†] Adam F. Chrimes,[†] Majid Mortazavi,[‡] David D. Yao,[†] Matthew R. Field,[§] Kay Latham,[§] Vipul Bansal,[§] James R. Friend,[†] Serge Zhuiykov,[⊥] Nikhil V. Medhekar,[‡,*] Michael S. Strano,[∥] and Kourosh Kalantar-zadeh[†,*]

[†]School of Electrical and Computer Engineering, RMIT University, Melbourne, Victoria, Australia, [‡]Department of Materials Engineering, Monash University, Clayton, Victoria, Australia, [§]School of Applied Sciences, RMIT University, Melbourne, Victoria, Australia, [⊥]Division of Materials Sciences and Engineering, CSIRO, Highett, Victoria, Australia, and [∥]Department of Chemical Engineering, Massachusetts Institute of Technology, Cambridge, Massachusetts 02139, United States. [#]These authors contributed equally to this work.

ABSTRACT Two-dimensional (2D) transition metal dichalcogenide semiconductors offer unique electronic and optical properties, which are significantly different from their bulk counterparts. It is known that the electronic structure of 2D MoS_2, which is the most popular member of the family, depends on the number of layers. Its electronic structure alters dramatically at near atomically thin morphologies, producing strong photoluminescence (PL). Developing processes for controlling the 2D MoS_2 PL is essential to efficiently harness many of its optical capabilities. So far, it has been shown that this PL can be electrically or mechanically gated. Here, we introduce an electrochemical approach to actively control the PL of liquid-phase-exfoliated 2D MoS_2 nanoflakes by manipulating the amount of intercalated ions including Li^+, Na^+, and K^+ into and out of the 2D crystal structure. These ions are selected as they are crucial components in many bioprocesses. We show that this controlled intercalation allows for large PL modulations. The introduced electrochemically controlled PL will find significant applications in future chemical and bio-optical sensors as well as optical modulators/switches.

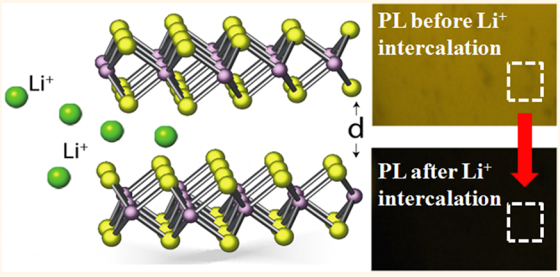

KEYWORDS: 2D materials · MoS_2 · liquid exfoliation · photoluminescence · ion intercalation

The 2H MoS_2 is an indirect band gap semiconductor with an energy gap of ~1.2 eV in its bulk form.[1,2] Owing to its unique layered structure, 2H MoS_2 has traditionally been used for various applications including photocatalysis,[3] solid-state lubrication,[4] hydrogen storage,[5] and in lithium ion batteries.[6] In principle, the bulk 2H MoS_2 is composed of covalently bonded S−Mo−S planes, which form 2D layers held together by van der Waals forces.[1,2,7] The van der Waals forces are weak enough to allow exfoliation to minimum resolvable monolayers, through externally applied forces. These monolayers show many interesting properties such as enhanced charge carrier mobility when placed in the vicinity of highly permittive boundaries, mechanical behavior along the plane that is different from their bulk counterparts and high surface-to-volume ratio for sensing applications.[1,2,8−15] It has been shown that the band gap of relatively large flakes of 2D MoS_2 increases with decreasing crystal thickness below 100 nm and eventually reaches ~1.9 eV for a monolayer.[16] Simultaneously, the band gap also changes from indirect to direct due to the hybridization between p_z orbitals of S atoms and d orbitals of Mo atoms.[16] Such an indirect-to-direct band gap transition leads to a strong photoluminescence (PL) effect in monolayer MoS_2. More recently, a new optical phenomenon has been demonstrated by Stengl and Henych where 2D MoS_2 nanoflakes with small lateral dimensions produce strong luminescence under UV light, which has been associated with the quantum confinement effect across the 2D planes.[17] Due to such characteristics, 2D MoS_2 flakes demonstrate distinguishing features in striking contrast to their bulk counterpart and are attractive for developing high-performance optical devices including optical sensors,

* Address correspondence to jianzhen.ou@rmit.edu.au, kourosh.kalantar@rmit.edu.au, nikhil.medhekar@monash.edu.

Received for review August 12, 2013 and accepted October 22, 2013.

Published online October 22, 2013
10.1021/nn4041987

© 2013 American Chemical Society

optical modulators, solar cells, and light-emitting diodes (LEDs).[1] The key for developing future applications of 2D MoS_2 and other transition metal dichalcogenides in general is to find different ways of controlling their physical properties. In particular, the focus of this paper is to offer a means to electrochemically control their PL on demand.

Applying changes to the surrounding electric field distribution has been shown to be an efficient method to modulate and ultimately gate the 2D MoS_2 band structure and hence its luminescent properties. Luminescence of 2D MoS_2 can be electrically altered and gated with large applied voltages.[18,19] As a result, by applying a high electric field, it is possible to adjust and modulate the PL.[19] This effect is ascribed to the interaction of excitons with charge carriers due to the phase-space-filling effect. Furthermore, PL in 2D MoS_2 can be adjusted by pumping circularly polarized light.[20,21] Additionally, it is known that the PL of stratified MoS_2 can be tuned by altering the number of stacked monolayers, hence providing a base for their active control.[16,22] However, it is practically a significant challenge to reversibly place the exfoliated monolayers in-registry atop each other.

It is recognized that ion intercalation modulation is an efficient way to change the band structure of bulk MoS_2. The electronic structure of MoS_2 can be electrochemically tuned, and indeed, there is vast literature on the electrochemical intercalation of bulk MoS_2.[6,23] There are also recent reports demonstrating the electrochemical transduction modulation in field effect transistors based on 2D MoS_2.[24,25]

In this work, we hypothesize that electrochemical means, which operate based on the diffusion of intercalating ions using applied voltages against a reference electrode, can be employed to tune the PL in 2D MoS_2. This facile method is used for actively controlling/modulating the PL in liquid-phase-exfoliated 2D MoS_2 nanoflakes by electrochemical intercalation/deintercalation of Li^+, Na^+, and K^+ ions. These ions are selected as it is known that they play vital roles in living cells[26] as well as many optical systems.[27] We show how these intercalated ions modify the crystal phase and electronic band structures of 2D MoS_2, eventually resulting in the loss of the material's semiconducting properties due to the emergence of a metallic phase. In particular, the theoretical calculations are demonstrated and discussed for the operation principle of Li^+ ion intercalation, the changes in the band structure, and consequently the PL.

RESULTS AND DISCUSSION

Synthesis and Characterization of 2D MoS_2 Nanoflakes. Many investigations regarding the optical properties of 2D MoS_2 employ mechanical exfoliation techniques, which can produce high-quality planar MoS_2 crystals.[16,18,22] The low yield is the major disadvantage of these mechanical techniques, realistically preventing their use in large-scale fabrication of a MoS_2-based PL system.[1,2,28,29] Vapor synthesis techniques have been proposed to tackle this issue, though they require high processing temperatures (700−1000 °C) incompatible with broadly available integrated circuit fabrication processes.[30,31] In addition, the nanostructured MoS_2 film matrix necessary to ensure effective interaction with photons and consequently high intensity modulation in an optical system is generally not possible using vapor synthesis techniques.

Liquid-phase exfoliation techniques, however, offer routes to practical mass synthesis of 2D materials at relatively low temperatures.[28,32−35] Early liquid-phase exfoliation techniques mainly involved the ion-assisted exfoliation processes, which are generally time-consuming, sensitive to environment, hazardous, and embed impurities.[1,2,36] Coleman *et al.* proposed the liquid-phase exfoliation of 2D MoS_2 flakes in an appropriate organic solvent with the aid of sonication.[37] This method yields large quantities of 2D MoS_2 flakes made of several monolayers demonstrated to produce moderate to strong PL.[28] It should be considered that the 2D MoS_2 flakes obtained in liquid-phase intercalation processes are generally small in lateral dimensions. Subsequently, their optical properties should be fully studied to ensure correct data are obtained.

The 2D MoS_2 nanoflakes used here are prepared using a grinding-assist liquid-phase exfoliation technique similar to that reported by Yao *et al.*[32] Details are presented in the Methods section. In brief, the commercial MoS_2 powder is mechanically ground with the *N*-nethyl-2-pyrrolidone (NMP) solvent and processed with high-power sonication. The supernatant containing 2D MoS_2 nanoflakes is collected after centrifugation. Atomic force microscopy (AFM) is used for assessing the lateral dimensions and thicknesses of these 2D MoS_2 layers. As can be seen in Figure 1a,b, a clear step of ∼3.6 nm (corresponding to 5−6 monolayers of MoS_2) can be observed in a typical 2D liquid-exfoliated MoS_2 flake with large lateral size of ∼50−100 nm. However, the lateral dimensions of these 2D nanoflakes are generally found to be less than 80 nm with the majority in the 10 to 40 nm region. The lateral distribution of the nanoflakes is shown in Figure 1c. It is also seen that the 2D nanoflakes have various thicknesses, but the majority consists of 2 to 7 monolayers (Figure 1d and Supporting Information Figure S1).

The crystal structure of these 2D nanoflakes is investigated using the X-ray diffraction (XRD) system, while the MoS_2 powder is used as the reference. From the XRD pattern shown in Figure 1e, it can be observed that both the 2D MoS_2 nanoflakes and bulk powder are identified as 2H MoS_2 with a dominant peak appearing at 14.4°, reflecting the (002) plane (ICDD card no. 77-1716). Interestingly, the exfoliated 2D nanoflakes

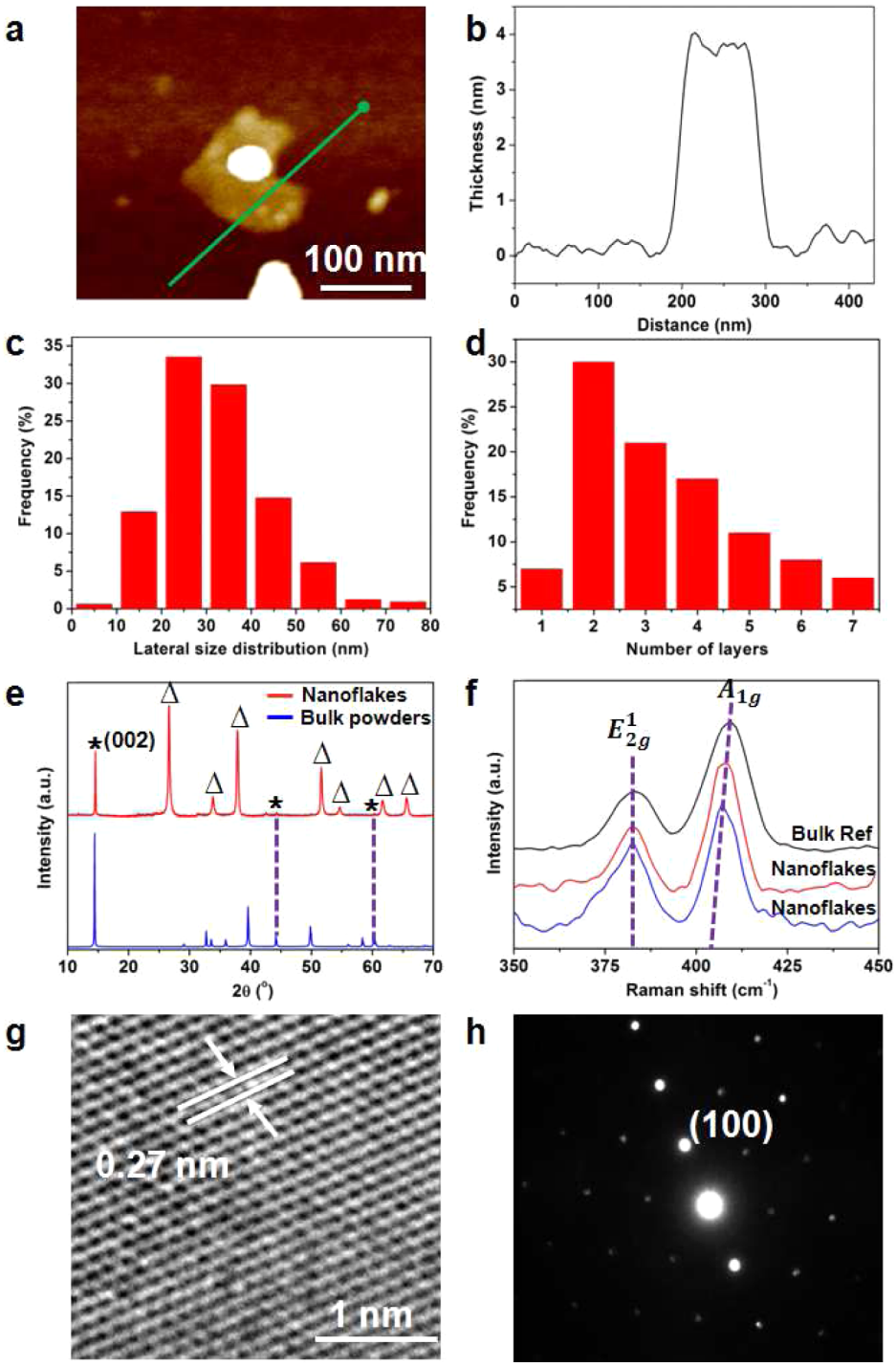

Figure 1. Characterization of 2D MoS_2 nanoflakes. (a) AFM image of a typical 2D MoS_2 flake. (b) Height profile along the green line overlaid on the image. (c) Lateral size of the 2D nanoflake distribution. (d) Thickness distribution of the 2D nanoflakes. (e) XRD patterns of 2D MoS_2 flakes and bulk powders both drop-casted onto FTO substrates (peaks correspond to [*] 2H MoS_2 and [Δ] FTO). (f) Raman spectra of bulk MoS_2 powder (black line) and 2D MoS_2 nanoflakes (red and blue lines), indicating both E^1_{2g} and A_{1g} Raman modes. (g) HRTEM image of a sample area of a 2D MoS_2 nanoflake and (h) its corresponding SAED pattern.

are found to have enhanced planar crystal structure in comparison to that of bulk counterpart, due to the relative increase in the peak intensity corresponding to the (002) plane.

Raman spectroscopy is also utilized here to further investigate the crystal structure and thickness of the 2D MoS_2 nanoflakes. From Figure 1f, two distinguished Raman peaks can be found at ~384 and ~406 cm^{-1} for the MoS_2 nanoflakes, corresponding to in-plane (E^1_{2g}) and vertical plane (A_{1g}) vibrations of Mo−S bonds in 2H MoS_2, respectively.[30,38] By normalizing both the Raman spectra taken from the bulk powder and nanoflakes with the E^1_{2g} mode, it is found that the 2D nanoflakes have a smaller Raman shift difference between E^1_{2g} and

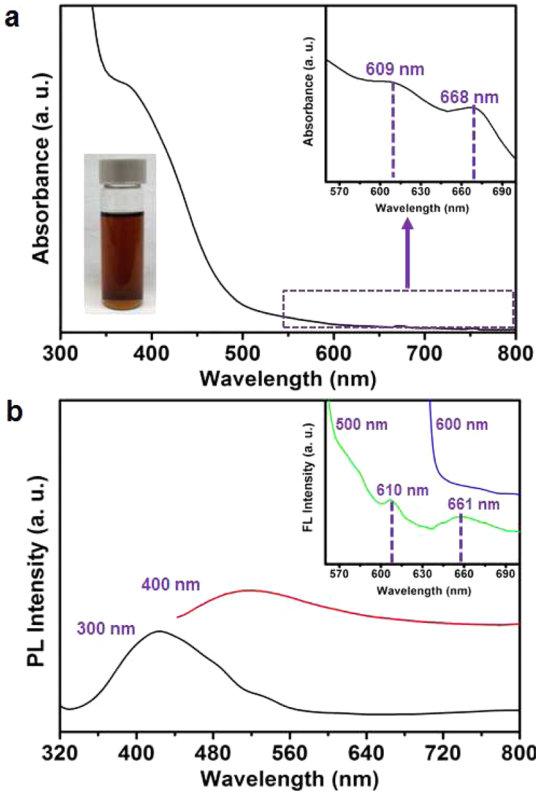

Figure 2. Optical and PL properties of 2D MoS_2 nanoflakes. (a) Absorbance spectrum of 2D MoS_2 nanoflakes (insets are the optical image of a liquid-exfoliated MoS_2 suspension in NMP solvent and its zoomed in region of the same spectrum showing two absorption peaks at 609 and 668 nm). (b) PL spectra of 2D MoS_2 nanoflakes at different excitation wavelengths (300, 400, 500, and 600 nm).

A_{1g} modes (Δ = ~22 cm^{-1}) in comparison with Δ = ~26 cm^{-1} from their bulk counterpart. Using information provided by Li *et al.*,[38] the Raman spectra indicate that the thicknesses of 2D MoS_2 nanoflakes are mostly less than 5 monolayers (<~3.5 nm) based on the frequency shift of the A_{1g} Raman mode, which is consistent with the AFM measurements (Figure 1d).

The crystal structure of MoS_2 is also revealed by using high-resolution transmission electron microscopy (HRTEM). Figure 1g shows the HRTEM image of a sample area of a 2D MoS_2 nanoflake. A lattice fringe spacing of 0.27 nm is identified in this image, which corresponds to the (100) lattice plane. The HRTEM images of the edges of flakes, such as the one presented in Figure S2, confirms the presence of perfectly 2D structures with the number of layers less than 5−6 monolayers. Figure 1h depicts the selected area electron diffraction (SAED) pattern of this region, which is indexed to the near perfect planar 2H MoS_2.

Optical Properties of 2D MoS_2 Nanoflakes. The supernatant containing a high concentration of 2D MoS_2 nanoflakes appears to be amber in color, as shown in the inset image in Figure 2a. The detailed optical properties of the nanoflakes are studied by measuring their UV−vis−NIR absorption spectra (Figure 2a). The weak absorption peaks at 609 and 668 nm are ascribed to B and A excitonic peaks, respectively, arising from the K point of the Brillouin zone in 2D MoS_2 with large lateral dimensions.[16] The weak features of these peaks are due to the small concentration of the relatively larger 2D flakes in the suspension (as evidenced in Figure 1c). In addition to these two weak peaks, an obvious broad peak centered at ~400 nm is observed. There is also a less prominent shoulder seen at 500 nm. It has been suggested that the optical absorption of low-dimensional or quantum dot MoS_2 exhibits a strong blue shift when the lateral dimensions of the MoS_2 nanostructures are reduced to <50 nm, ascribed to the quantum size effect.[39−42] As the majority of our 2D flake sizes are within 10−40 nm range (Figure 1c), their optical absorption peaks should also be blue-shifted. In addition, the broad absorption peak below 350 nm can be assigned to blue-shifted convoluted Z, C, and D excitonic peaks as suggested by several researchers.[40−42]

The PL spectra using fluorescence spectroscopy at four different excitation wavelengths of 600, 500, 400, and 300 nm are measured to provide a comprehensive view of the PL properties of the 2D nanoflakes. While no obvious emission peak is observed at the excitation wavelength of 600 nm (inset in Figure 2b), two weak peaks at ~610 and ~661 nm can be seen (inset in Figure 2b) when the excitation wavelength is 500 nm. It is well-known that the observed peaks are mainly from the direct band gap hot PL from the K point of the 2D MoS_2 flakes with the large lateral dimensions.[16] However, when the excitation energies are larger (at lower wavelengths of 400 and 300 nm), a strong broad peak centered at ~420 nm and a weaker shoulder at 530 nm appear. In this case, the characteristics of these PL peaks are similar to those of MoS_2 quantum dots or liquid-exfoliated 2D MoS_2 with small lateral dimensions, which are ascribed to the strongly blue-shifted hot PL from the K point.[17,29] Some comparable results are recently presented by Stengl and Henych, who carefully studied such a phenomenon.[17] Similarly, they obtained 2D MoS_2 nanoflakes of various lateral dimensions, with the mean value of ~30 nm, using liquid-phase exfoliation techniques. They showed that the increase in the excitation wavelength from 350 to 550 nm red-shifted the luminescent peaks from nearly 440 to 600 nm due to the polydispersity of the nanoflakes. Interestingly, similar phenomena were observed in our nanostructured MoS_2 film consisting of 2D nanoflakes under the excitation of the light sources with various wavelengths (Figure S3).

Active Control of the PL in 2D MoS_2 Nanoflakes and the Characteristics. The confirmation of the aforementioned optical characteristics of the 2D MoS_2 nanoflakes at multiple excitation wavelengths provides a preliminary base for understanding the fundamentals of the PL generated by our 2D MoS_2 nanoflakes. Here we

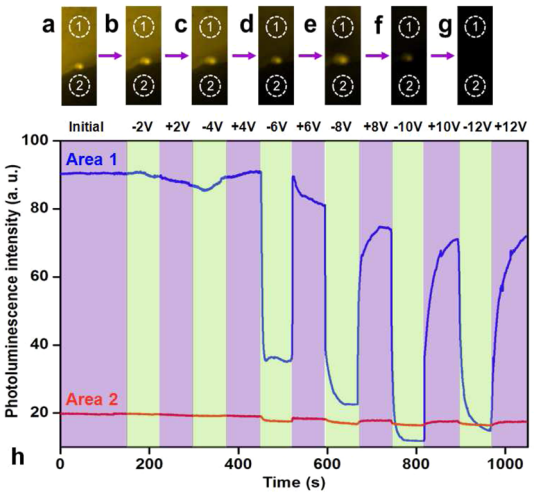

Figure 3. Active control of PL in the 2D MoS_2 nanoflakes. PL images of the nanostructured MoS_2 film at the intercalating voltages of (a) 0 V, (b) −2 V, (c) −4 V, (d) −6 V, (e) −8 V, (f) −10 V, and (g) −12 V. (h) *In situ* PL intensity change of a selected area "1" in the MoS_2 film under different intercalating/deintercalating voltages of ±2, ±4, ±6, ±8, ±10, and ±12 V in the 0.1 M $LiClO_4$ solution (blue line) at the step duration of 60 s, while a selected uncoated area "2" within the substrate area is chosen as the reference (red line).

demonstrate that upon the intercalation/deintercalation of Li^+, Na^+, and K^+ ions the PL intensities can be effectively tuned. In order to establish the system for investigating the interaction with ions, the 2D MoS_2 supernatant was drop-casted onto conductive fluorine-doped tin oxide (FTO) substrates to obtain nanostructured thin films with the thicknesses of ∼1 μm. Epifluorescence microscopy, with the specific area selection specificity, was utilized for *in situ* measurement of the PL intensities of the films, while the PL intensity of the uncovered substrate was used as the reference. The microscope operated at a blue excitation light source covering the wavelengths ranging between 400 and 500 nm (the detailed schematic of experimental setup is shown in Figure S4).

The Li^+ ion intercalation is presented in detail. During the intercalation process, an external voltage is applied across the working cathode (FTO coated with the 2D MoS_2 nanoflake film) and the counter electrode (Pt). It is known that, in bulk MoS_2, this leads to the intercalation of the x quantity ($0 \le x \le 1$) of Li^+ ions and injection of an equal quantity of electrons (e^-) into MoS_2.[23] This double intercalation/injection of charges results in the formation of Li_xMoS_2, hence leading to the modification of their original crystal phase (from trigonal prismatic 2H to octahedral 1T phase) and electronic band structures.[23,43] Conversely, when the polarity of the applied voltages is reversed, Li^+ ions are deintercalated, which leads to the restoration of the initial crystal phase and electronic band structures (this will be further discussed in a later section).

The intercalation is investigated using voltages from −2 to −12 V in −2 V steps and duration of 60 s (Figure 3a−g). The dynamic response of the PL in a specific area (annotated as "1") of the MoS_2 film at different intercalating/deintercalating voltages is presented in Figure 3h. It can be seen that there are only small PL modulations at the applied voltages of −2 and −4 V, possibly due to insufficient electric field force for inserting Li^+ ions into MoS_2. Interestingly, at −6 V, a significant PL modulation of ∼61% at a short response time of ∼4 s is observed (definition of PL modulation, response and recovery time, as well as reversibility are presented in Supporting Information). Decreasing the intercalating voltage further results in a larger PL modulation, while the response time remains below 20 s. The complete quenching occurs at the intercalating voltage of −10 V in which the PL intensity of the nanostructured MoS_2 film is lower than that of the reference substrate. For intercalating voltages of <−10 V, the PL modulation does not increase further and the response time is prolonged to >20 s. This possibly indicates that a significant amount of the intercalated Li^+ ions are trapped in the sites close to the MoS_2/electrolyte interface, instead of being diffused deeper. In addition, the overall recovery kinetics at different deintercalating voltages are excellent as their recovery time are less than 40 s with a reversibility larger than 0.9. It is noted that there is a sudden drop in the PL intensity during the application of a deintercalating voltage of +6 V. Possibly some of the stacked 2D flakes from the MoS_2 film are detached in the presence of the moderate electric field force.

In addition to Li^+ ions, Na^+ and K^+ ions are also used as for electrochemically controlling the PL of 2D MoS_2 nanoflakes. As seen from Figure 4a−c and Figure S5, the PL modulation starts from −4 V for both Na^+ and K^+ ion intercalation similar to the Li^+ ion intercalation case. For Na^+ ions, the optimum intercalating voltage is found to be at −8 V, where ∼65% PL modulation is achieved with a small response and recovery time of ∼10 and ∼20 s, respectively. It is found that the PL modulation induced by K^+ ion intercalation is only up to ∼40% at an optimum intercalating voltage of −10 V, which is only half in comparison to that of Li^+ ions, possibly due to their slow diffusivity owing to their relatively larger dimension (Figure 4a−c and Figure S5). Despite the reduction of PL modulation, it demonstrates relatively short response and recovery time, which both are under ∼10 s when the intercalating voltages are smaller than −12 V. It is observed that the recovery time is dramatically increased to ∼40 s at −12 V, which is probably due to the deep entrapments of ions in the MoS_2 structure at such voltages.

The PL modulations of the 2D MoS_2 nanoflakes can be directly ascribed to the ion intercalation into the MoS_2 crystal structure. For case of the Li^+ ions, it is suggested that the intercalated Li^+ ions are weakly bonded to the S atoms of the MoS_2 layers and placed in the van der Waal's gap between the MoS_2 planes when

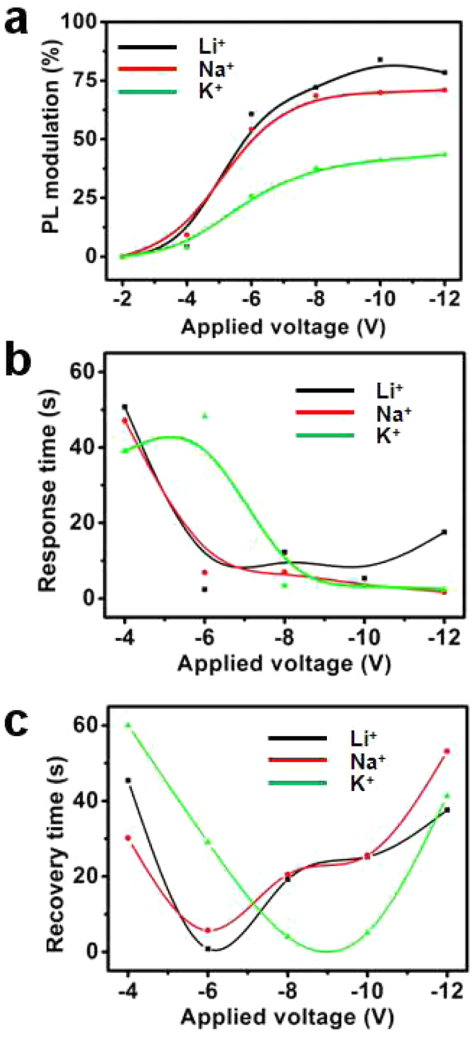

Figure 4. Active control of PL in the 2D MoS_2 nanoflakes using different ions. Comparison of (a) PL modulations, (b) response time, and (c) recovery time of the nanostructured MoS_2 film after Li^+, Na^+, and K^+ ion intercalation (B-spline is used for the graphs).

more than one monolayer exists.[23,44] For such a multiple layer system, this results in the lattice expansion and a decrease in the overall van der Waals forces between the planes, as illustrated in the inset of Figure 5a.[23,44] It has been suggested that high concentration of these intercalating Li^+ ions eventually forces the transition of the MoS_2 crystal from stable hexagonal semiconducting phase (2H phase) to a metastable metallic phase (1T phase).[28,45−48] Such a phase transition can be evidenced by X-ray photoelectron spectroscopy (XPS) measurements shown in Figure 6. According to Figure 6a−c, $Mo3d_{3/2}$, $Mo3d_{5/2}$, S2s, $S2p_{1/2}$, and $S2p_{3/2}$ peaks can be observed at 232.5, 229.3, 226.5, 163.7, and 162.2 eV, respectively, indicating the dominant 2H MoS_2 phase in the crystal structure of pristine 2D MoS_2 nanoflakes.[49] After Li^+ ion intercalation at −10 V, new peaks at 230.9 and 227.7 eV for Mo and 162.8 and 161.3 eV for S can be found at lower binding energies in comparison with those of 2H phase peaks (Figure 6e,f). These new peaks can be identified as 1T phase peaks, which suggests that a large portion of the 2D MoS_2 flakes undergoes a phase transition to a metastable phase, where the coordination of Mo atoms becomes octahedral (1T phase) upon Li^+ ion intercalation.[49] However, the peaks representing the 2H phase can still be observed after the intercalation process, indicating the coexistence of 1T and 2H phases in the crystal structure of intercalated material. Such a 2H → 1T phase transition can be one of the main reasons that contribute to the PL quenching of 2D MoS_2 nanoflakes, as the 1T phase appears to be metallic.[28,43] It is also noticed that a small peak appears at 236.0 eV (Figure 6e), corresponding to Mo^{6+} $3d_{5/2}$, which is a common characteristic for Li^+-intercalated MoS_2 possibly due to the oxidation of a very small portion of MoS_2.[50] The deintercalation process of Li^+ ions results in the near full restoration of the 2H phase crystal structure in 2D MoS_2 nanoflakes, with less than 15% of 1T phase and a very small portion of residual Li^+ ions remaining within the overall crystal structure (Figure 6g−i).

First principles calculations are used for assessing the changes of the spacing between the layers and alteration of the band structure at various degrees of ion intercalation. It is important for the readers to consider that the simulations do not include the quantum confinement effect. They rather show the alteration of the layer spacing and electronic structure in an ideal 2D MoS_2 system after the intercalation. Additionally, the incorporation of the quantum confinement effect in such calculations is beyond our current computational capabilities. The calculations are conducted on both 2H and 1T MoS_2 bilayer systems upon Li^+ ion intercalation as a close representative to the measurements. As expected, the intercalation of Li^+ ions increases the distance between the two 2D MoS_2 planar monolayers forming Li_xMoS_2 for both crystal phases. For the 2H phase, the interlayer distance (d) rapidly increases from ∼3.1 Å for pristine MoS_2 bilayer to ∼3.4 Å for $Li_{0.125}MoS_2$, as shown in Figure 5a. As the concentration of intercalated Li^+ ions increases, d keeps increasing but at a much slower rate, and finally, the spacing reaches ∼3.5 Å for $Li_{0.5}MoS_2$. By taking account of the 2H → 1T crystal phase transition into the calculation, there is a rapid jump of d from ∼3.0 to 3.5 Å at the mild Li^+ ion intercalation level (1T $Li_{0.125}MoS_2$). However, afterward, d is continuously reduced and eventually reaches ∼3.3 Å for 1T $Li_{0.5}$-MoS_2. The increases in the interlayer distances in both 2H and 1T cases affect the electronic band structures of the corresponding intercalated compounds, which will be discussed later (Figure 5b).

Characterizations are conducted to assess the intercalation of ions into 2D MoS_2. For brevity, the measurements are limited to Li^+ ion intercalation. In order to monitor the effects of Li^+ ion intercalation in time into

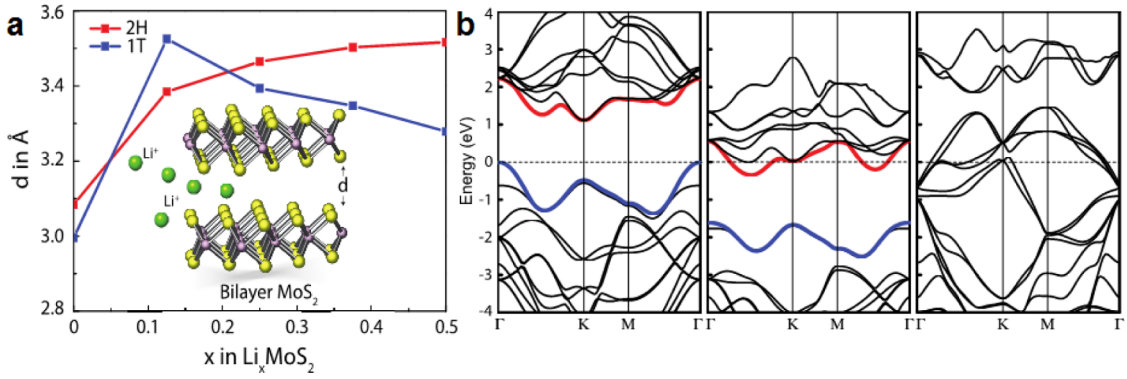

Figure 5. DFT calculations for a bilayer 2D MoS_2 nanoflake before and after Li^+ ion intercalation. (a) Schematic of lattice structure of layered MoS_2 upon Li^+ intercalation in bilayer 2H and 1T MoS_2 as well as the change in the spacing between the two planes upon the Li^+ intercalation at different amounts. (b) Calculated electronic band structures of bilayer (left) pristine MoS_2, (middle) 2H $Li_{0.5}MoS_2$, and (right) 1T $Li_{0.5}MoS_2$. The Fermi level is set to zero in each case.

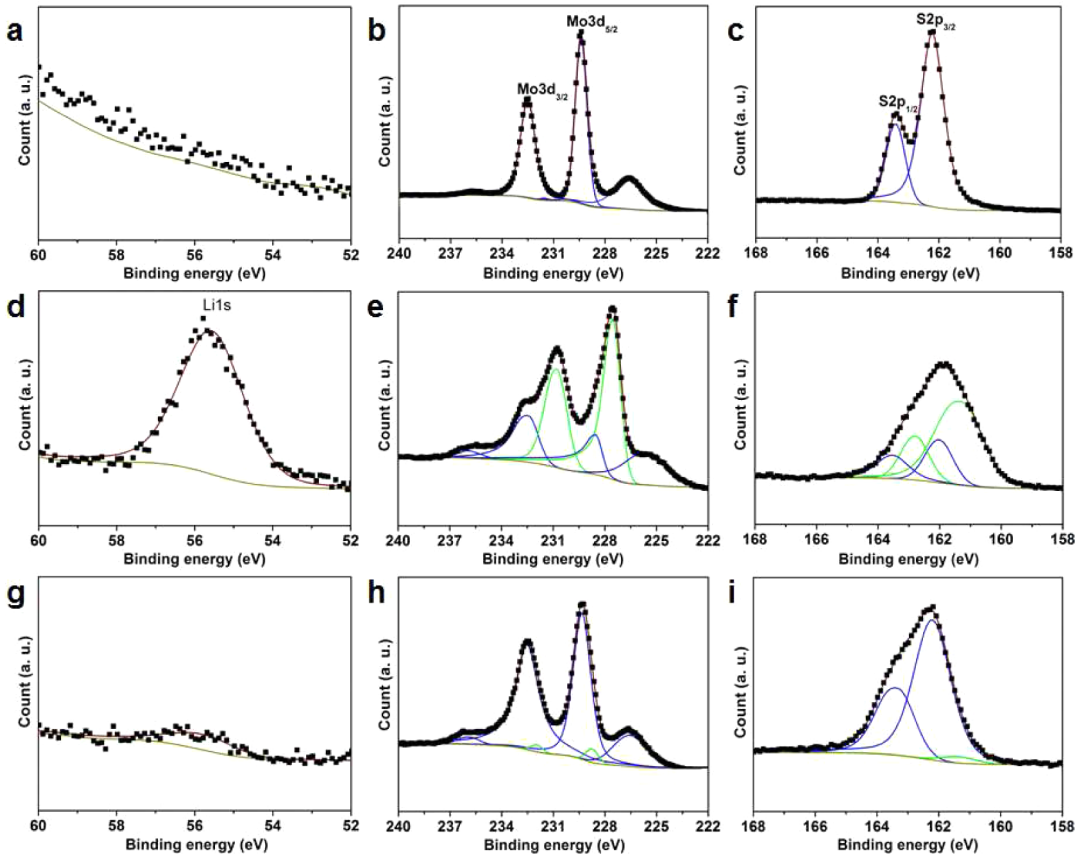

Figure 6. Characterization of 2D MoS_2 nanoflakes after Li^+ ion intercalation and deintercalation. XPS spectra of the elements of (a) Li, (b) Mo, and (c) S in 2D MoS_2 nanoflakes before Li^+ ion intercalation. (d–f) Aforementioned elements in 2D MoS_2 nanoflakes after Li^+ ion intercalation, where the blue and green lines represent the 2H and 1T phase, respectively. (g–i) Three elements in 2D MoS_2 nanoflakes after Li^+ ion deintercalation.

the 2D MoS_2 nanoflakes, *in situ* Raman spectroscopy is used. Figure 7a shows that both E^1_{2g} and A_{1g} Raman modes are observed to shift to the right, indicating an increase in the vibration frequency, with respect to the initial Raman spectrum. The shift in A_{1g} mode, corresponding to vertical plane vibrations of Mo–S bonds, is observed to be much larger than that of E^1_{2g} mode, which represents the in-plane vibrations. The peak shift observed in the Raman spectrum can be related to the strain introduced in the lattice and the effect of increased van der Waals forces from the intercalating Li^+ ions suppressing the vibrations of Mo–S bonds.[30] This also explains the increased stiffening of the vertical vibration modes compared to the in-plane vibrations.[23] In addition, there is a significant reduction in the intensities of both Raman modes for the

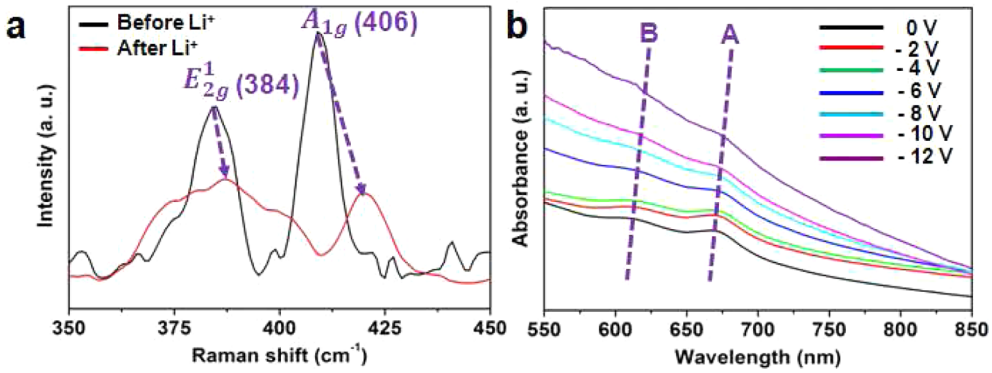

Figure 7. Characterization of 2D MoS_2 nanoflakes after Li^+ ion intercalation. (a) *In situ* Raman spectra of 2D MoS_2 nanoflakes before and after Li^+ intercalation at an intercalating voltage of −10 V. (b) *In situ* absorbance spectra of large 2D MoS_2 nanoflakes at the intercalation voltages of 0, −2, −4, −6, −8, −10, and −12 V.

intercalated MoS_2 Raman spectrum compared to that of the pristine 2D MoS_2 nanoflakes, indicating the crystal transformation from original 2H MoS_2 into intercalated Li_xMoS_2 ($x < 0.5$). Furthermore, the E^1_{2g} mode is significantly broadened in comparison to the A_{1g} mode after the intercalation of Li^+ ions, further confirming the presence of Li_xMoS_2 ($x < 0.5$).[23]

While the vibrational properties of the 2D MoS_2 crystal structure is confirmed to be altered by the Li^+ ion intercalation, the concomitantly injected electrons during the intercalation process behave as Drude-model-like free electrons and eventually enter into the MoS_2 band structure, producing the additional electronic states.[2] Such additional electronic states in both intercalated 2H and 1T crystal phases are therefore believed to be another main reason to cause the PL quenching of 2D MoS_2 nanoflakes.

In order to verify the aforementioned hypothesis, *in situ* absorbance measurements are conducted. In these experiments, only MoS_2 A (~668 nm) and B (~609 nm) excitonic peaks are investigated by focusing on the behavior of flakes with relatively large lateral dimensions, as their alterations can be well-described using the first principles calculations. While the majority of PL generated by our 2D materials is due to the quantum confinement effect of 2D flakes with small lateral dimensions, such a measurement and relevant theoretical discussions are still mostly applicable. This is due to the fact that the peaks of the smaller flakes are also the same A and B excitonic peaks, which are blue-shifted. From Figure 7b, it can be seen that both absorbance resonance peaks are gradually suppressed with the increase of the intercalating voltage, and there is a slight red shift in both peaks when the intercalating voltage is smaller than −6 V. Both phenomena suggest that the electronic band structure of 2D MoS_2 is modified upon the Li^+ ion intercalation.[28] This manipulation of electronic structure can be, in principal, observed in the first principle calculations shown in Figure 5b for the bilayer structure with both intercalated 2H and 1T crystal phases. For the case of the intercalated 2H phase, the calculated structures demonstrate that Li^+ ion intercalation causes a downshift of the conduction band due to the existence of additional electronic states. These states are formed by the concomitantly injected electrons during the intercalation process, producing metallic Li_xMoS_2. For the 1T crystal phase, in addition to the concomitantly injected electrons similar to the 2H phase case, the other origin of this phenomenon can be ascribed to the presence of Mo4d state, forming a band that hosts the Fermi level.[43,46] Both cases indicate that the bilayer MoS_2 exhibits a semiconductor-to-metal transition upon the Li^+ ion intercalation, which represents the key to cause the PL quenching of 2D MoS_2 nanoflakes.

CONCLUSION

A facile and reliable approach was introduced to actively control the PL in the liquid-phase-exfoliated 2D MoS_2 nanoflakes by electrochemically manipulating the amount of intercalating Li^+, Na^+, and K^+ ions into the MoS_2 crystal structure. This kind of controlling process was demonstrated to allow for large PL modulations, short response and recovery times, as well as excellent reversibility. The intercalations of these ions led to the lattice expansion in MoS_2 as well as the transformation of a significant portion of the crystal from originally 2H into 1T crystal phase. This consequently resulted in the alternation of the electronic band structure, exhibiting a semiconducting to metallic state transition, which contributed to the PL quenching. We also demonstrated that the 2H MoS_2 crystal phase was almost restored after the deintercalation of ions.

This reversible controlling approach will provide a viable solution to develop a high performance and practical nanostructured PL system based on 2D MoS_2 with active controllability. The demonstrated phenomenon can also play an important role in developing highly sensitive photoelectrochemical sensors as well

as high-performance optical modulators and solar cells. Additionally, this controlled PL will also offer great opportunities for the development of optical displays and switches at relevant wavelengths.

METHODS

Two-Dimensional MoS_2 Nanoflake Preparation and Characterization. One gram of MoS_2 powders (99% purity, Sigma Aldrich) was added to 0.5 mL of NMP (99% anhydrous, Sigma Aldrich) in a mortar and ground for 30 min. The mixture was placed in a vacuum oven to dry overnight at room temperature, then was collected and redispersed into a 10 mL NMP solvent. The solution was probe-sonicated (Ultrasonic Processor GEX500) for 90 min at the power of 125 W, and the supernatant containing 2D MoS_2 nanoflakes was collected after being centrifuged for 45 min at the speed of 4000 rpm. Lateral dimensions and thickness of these 2D nanoflakes were measured using AFM (Bruker Multimode 8 with PF TUNA). Their crystal structure was characterized using XRD (Bruker D8 DISCOVER), HRTEM (JEOL 2100F), and Raman microscopy (Horiba TRIAX 320 spectrometer fiber coupled to an Olympus BX41 confocal microscope with 532 nm 90 μW excitation). XPS measurements were performed on a VG-310F instrument using Al non-monochromated X-rays (20 kV, 15 mA) with the hemispherical energy analyzer set at a pass energy of 20 eV for the peak scans. The absorbance spectra of the 2D nanoflakes were examined using a spectrophotometric system consisting of a Micropack DH-2000 UV−vis−NIR light source and an Ocean Optics HR4000 spectrophotometer. The PL spectra of the 2D nanoflakes were obtained from a Perkin−Elmer LS 55 luminescence spectrometer at multiple excitation wavelengths of 300, 400, 500, and 600 nm.

Active Control of PL in 2D MoS_2 Nanoflakes. One hundred microliters of the MoS_2 supernatant was drop-casted onto a conductive FTO substrate with the exposed area of ~0.5 cm^2 at ~60 °C. Various voltages ranged from ±2 to ±12 V were applied across a two-electrode configuration *via* a DC power supply where the cathode was connected to the drop-casted nanostructured MoS_2 film on FTO and the anode was a Pt wire. The electrolytes were 0.1 M $LiClO_4$ (98% purity, Sigma Aldrich), 0.1 M $NaClO_4$ (98% purity, Sigma Aldrich), or 0.1 M KPF_6 (98% purity, Sigma Aldrich) in polypropylene carbonate (97% anhydrous, Sigma Aldrich). The PL intensities of the 2D nanoflakes were measured using a Nikon epifluorescence microscope with a blue excitation light source covering the wavelengths between 400 and 500 nm.

Computational Methods. The first principles calculations were performed within the framework of density functional theory (DFT) using the Vienna Ab initio Simulation Package.[50] The generalized gradient approximation of Perdew−Burke−Ernzerhof form was used to describe the exchange-correlation functional.[51] The core and valence electronic interactions were modeled through projector-augmented wave potentials.[52] The electrons in $1s^2 2s^1$, $4p^6 5s^1 4d^5$, and $2s^2 3p^4$ states were treated as valence electrons for Li, Mo, and S, respectively. The kinetic energy cutoff of 600 eV and a 21 × 21 × 1 Γ-centered mesh for sampling Brillouin zone of the bilayer MoS_2 unit cell were used to ensure the variation in total energy is less than 1 meV/atom. Optimized lattice parameters were obtained by allowing cell vectors and ionic positions to fully relax until the Hellmann−Feynman forces were less than 0.01 eV/Å. For accurate band structure calculations, a 45 × 45 × 1 Γ-centered mesh was used for sampling the Brillouin zone. Finally, since the standard generalized gradient approximation does not include weak dispersion interactions,[53] Grimme's DFT-D2 energy correction method was employed to correctly describe interlayer van der Waals interactions.[54,55] With this correction, the obtained interlayer distance in pure bilayer MoS_2 was 3.08 Å, in close agreement with experimentally measured value of 2.985 Å.[56] To study the effect of Li^+ ion intercalation, a 2 × 2 bilayer supercell was considered for both 2H and 1T MoS_2 polytypes. Li^+ ions were sequentially introduced in the low-energy octahedral binding sites, and the intercalated bilayer structure was again optimized.

Conflict of Interest: The authors declare no competing financial interest.

Acknowledgment. We would like to thank Prof. Michael Fuhrer (Monash University, Australia) regarding the discussion on the photoluminescence section in the manuscript. The authors also gratefully acknowledge the facilities, and the scientific and technical assistance of the Australian Microscopy & Microanalysis Research Facility at the RMIT Microscopy & Microanalysis Facility, at RMIT University. M.M. and N.M. acknowledge the computational support from MASSIVE, IVEC, and the Australian National Computing Infrastructure.

Supporting Information Available: More characterization of 2D MoS_2 nanoflakes using AFM; HRTEM image of a 2D MoS_2 flake; fluorescent images of the nanostructured MoS_2 thin film when excited by different light sources; experimental setup of the *in situ* PL intensity measurements; *in situ* PL intensity changes of the MoS_2 film upon the intercalation/deintercalation of Li^+, Na^+, and K^+ ions; definitions of PL modulation, response and recovery times, as well as reversibility. This material is available free of charge *via* the Internet at http://pubs.acs.org.

REFERENCES AND NOTES

1. Wang, Q. H.; Kalantar-zadeh, K.; Kis, A.; Coleman, J. N.; Strano, M. S. Electronics and Optoelectronics of Two-Dimensional Transition Metal Dichalcogenides. *Nat. Nanotechnol.* **2012**, *7*, 699–712.
2. Balendhran, S.; Walia, S.; Nili, H.; Ou, J. Z.; Zhuiykov, S.; Kaner, R. B.; Sriram, S.; Bhaskaran, M.; Kalantar-zadeh, K. Two-Dimensional Molybdenum Trioxide and Dichalcogenides. *Adv. Funct. Mater.* **2013**, *23*, 3952–3970.
3. Xiang, Q.; Yu, J.; Jaroniec, M. Synergetic Effect of MoS_2 and Graphene as Cocatalysts for Enhanced Photocatalytic H_2 Production Activity of TiO_2 Nanoparticles. *J. Am. Chem. Soc.* **2012**, *134*, 6575–6578.
4. Chhowalla, M.; Amaratunga, G. A. J. Thin Films of Fullerene-like MoS_2 Nanoparticles with Ultra-low Friction and Wear. *Nature* **2000**, *407*, 164–167.
5. Chen, J.; Kuriyama, N.; Yuan, H.; Takeshita, H. T.; Sakai, T. Electrochemical Hydrogen Storage in MoS_2 Nanotubes. *J. Am. Chem. Soc.* **2001**, *123*, 11813–11814.
6. Dominko, R.; Arcon, D.; Mrzel, A.; Zorko, A.; Cevc, P.; Venturini, P.; Gaberscek, M.; Remskar, M.; Mihailovic, D. Dichalcogenide Nanotube Electrodes for Li-Ion Batteries. *Adv. Mater.* **2002**, *14*, 1531–1534.
7. Ramakrishna Matte, H. S. S.; Gomathi, A.; Manna, A. K.; Late, D. J.; Datta, R.; Pati, S. K.; Rao, C. N. R. MoS_2 and WS_2 Analogues of Graphene. *Angew. Chem., Int. Ed.* **2010**, *49*, 4059–4062.
8. Radisavljevic, B.; Radenovic, A.; Brivio, J.; Giacometti, V.; Kis, A. Single-Layer MoS_2 Transistors. *Nat. Nanotechnol.* **2011**, *6*, 147–150.
9. Ataca, C.; Sahin, H.; Akturk, E.; Ciraci, S. Mechanical and Electronic Properties of MoS_2 Nanoribbons and Their Defects. *J. Phys. Chem. C* **2011**, *115*, 3934–3941.
10. Kim, S.; Konar, A.; Hwang, W. S.; Lee, J. H.; Lee, J.; Yang, J.; Jung, C.; Kim, H.; Yoo, J. B.; Choi, J. Y.; *et al.* High-Mobility and Low-Power Thin-Film Transistors Based on Multilayer MoS_2 Crystals. *Nat. Commun.* **2012**, *3*, 1011.
11. Sup Choi, M.; Lee, G. H.; Yu, Y. J.; Lee, D. Y.; Hwan Lee, S.; Kim, P.; Hone, J.; Jong Yoo, W. Controlled Charge Trapping by Molybdenum Disulphide and Graphene in Ultrathin Heterostructured Memory Devices. *Nat. Commun.* **2013**, *4*, 1624.
12. Late, D. J.; Liu, B.; Matte, H.; Dravid, V. P.; Rao, C. N. R. Hysteresis in Single-Layer MoS_2 Field Effect Transistors. *ACS Nano* **2012**, *6*, 5635–5641.

13. Lopez-Sanchez, O.; Lembke, D.; Kayci, M.; Radenovic, A.; Kis, A. Ultrasensitive Photodetectors Based on Monolayer MoS_2. *Nat. Nanotechnol.* **2013**, *8*, 497–501.
14. Bahartan, K.; Gun, J.; Sladkevich, S.; Prikhodchenko, P. V.; Lev, O.; Alfonta, L. Encapsulation of Yeast Displaying Glucose Oxidase on Their Surface in Graphene Oxide Hydrogel Scaffolding and Its Bioactivation. *Chem. Commun.* **2012**, *48*, 11957–11959.
15. Li, J.; Medhekar, N. V.; Shenoy, V. B. Bonding Charge Density and Ultimate Strength of Monolayer Transition Metal Dichalcogenides. *J. Phys. Chem. C* **2013**, *117*, 15842–15848.
16. Mak, K. F.; Lee, C.; Hone, J.; Shan, J.; Heinz, T. F. Atomically Thin MoS_2: A New Direct-Gap Semiconductor. *Phys. Rev. Lett.* **2010**, *105*, 136805.
17. Stengl, V.; Henych, J. Strongly Luminescent Monolayered MoS_2 Prepared by Effective Ultrasound Exfoliation. *Nanoscale* **2013**, *5*, 3387–3394.
18. Sundaram, R. S.; Engel, M.; Lombardo, A.; Krupke, R.; Ferrari, A. C.; Avouris, P.; Steiner, M. Electroluminescence in Single Layer MoS_2. *Nano Lett.* **2013**, *13*, 1416–1421.
19. Newaz, A. K. M.; Prasai, D.; Ziegler, J. I.; Caudel, D.; Robinson, S.; Haglund, R. F., Jr.; Bolotin, K. I. Electrical Control of Optical Properties of Monolayer MoS_2. *Solid State Commun.* **2013**, *155*, 49–52.
20. Wu, S.; Ross, J. S.; Liu, G. B.; Aivazian, G.; Jones, A.; Fei, Z.; Zhu, W.; Xiao, D.; Yao, W.; Cobden, D.; *et al.* Electrical Tuning of Valley Magnetic Moment through Symmetry Control in Bilayer MoS_2. *Nat. Phys.* **2013**, *9*, 149–153.
21. Mak, K. F.; He, K.; Shan, J.; Heinz, T. F. Control of Valley Polarization in Monolayer MoS_2 by Optical Helicity. *Nat. Nanotechnol.* **2012**, *7*, 494–498.
22. Splendiani, A.; Sun, L.; Zhang, Y.; Li, T.; Kim, J.; Chim, C.-Y.; Galli, G.; Wang, F. Emerging Photoluminescence in Monolayer MoS_2. *Nano Lett.* **2010**, *10*, 1271–1275.
23. Julien, C.; Sekine, T.; Balkanski, M. Lattice Dynamics of Lithium Intercalated MoS_2. *Solid State Ionics* **1991**, *48*, 225–229.
24. Chakraborty, B.; Bera, A.; Muthu, D. V. S.; Bhowmick, S.; Waghmare, U. V.; Sood, A. K. Symmetry-Dependent Phonon Renormalization in Monolayer MoS_2 Transistor. *Phys. Rev. B* **2012**, *85*, 161403.
25. Ye, J. T.; Zhang, Y. J.; Kasahara, Y.; Iwasa, Y. Interface Transport Properties in Ion-Gated Nano-Sheets. *Eur. Phys. J.: Spec. Top.* **2013**, *222*, 1185–1201.
26. Cerda, B. A.; Wesdemiotis, C. Li^+, Na^+, and K^+ Binding to the DNA and RNA Nucleobases. Bond Energies and Attachment Sites from the Dissociation of Metal Ion-Bound Heterodimers. *J. Am. Chem. Soc.* **1996**, *118*, 11884–11892.
27. Lee, S. H.; Deshpande, R.; Parilla, P. A.; Jones, K. M.; To, B.; Mahan, A. H.; Dillon, A. C. Crystalline WO_3 Nanoparticles for Highly Improved Electrochromic Applications. *Adv. Mater.* **2006**, *18*, 763–766.
28. Eda, G.; Yamaguchi, H.; Voiry, D.; Fujita, T.; Chen, M.; Chhowalla, M. Photoluminescence from Chemically Exfoliated MoS_2. *Nano Lett.* **2011**, *11*, 5111–5116.
29. Zhou, K.; Zhu, Y.; Yang, X.; Zhou, J.; Li, C. Demonstration of Photoluminescence and Metal-Enhanced Fluorescence of Exfoliated MoS_2. *ChemPhysChem* **2012**, *13*, 699–702.
30. Balendhran, S.; Ou, J. Z.; Bhaskaran, M.; Sriram, S.; Ippolito, S.; Vasic, Z.; Kats, E.; Bhargava, S.; Zhuiykov, S.; Kalantar-zadeh, K. Atomically Thin Layers of MoS_2 *via* a Two Step Thermal Evaporation-Exfoliation Method. *Nanoscale* **2012**, *4*, 461–466.
31. Liu, K. K.; Zhang, W.; Lee, Y. H.; Lin, Y. C.; Chang, M. T.; Su, C. Y.; Chang, C. S.; Li, H.; Shi, Y.; Zhang, H.; *et al.* Growth of Large-Area and Highly Crystalline MoS_2 Thin Layers on Insulating Substrates. *Nano Lett.* **2012**, *12*, 1538–1544.
32. Yao, Y.; Tolentino, L.; Yang, Z.; Song, X.; Zhang, W.; Chen, Y.; Wong, C. P. High-Concentration Aqueous Dispersions of MoS_2. *Adv. Funct. Mater.* **2013**, *23*, 3577–3583.
33. Smith, R. J.; King, P. J.; Lotya, M.; Wirtz, C.; Khan, U.; De, S.; O'Neill, A.; Duesberg, G. S.; Grunlan, J. C.; Moriarty, G.; *et al.* Large-Scale Exfoliation of Inorganic Layered Compounds in Aqueous Surfactant Solutions. *Adv. Mater.* **2011**, *23*, 3944–3948.
34. Zhou, K. G.; Mao, N. N.; Wang, H. X.; Peng, Y.; Zhang, H. L. A Mixed-Solvent Strategy for Efficient Exfoliation of Inorganic Graphene Analogues. *Angew. Chem., Int. Ed.* **2011**, *50*, 10839–10842.
35. O'Neill, A.; Khan, U.; Coleman, J. N. Preparation of High Concentration Dispersions of Exfoliated MoS_2 with Increased Flake Size. *Chem. Mater.* **2012**, *24*, 2414–2421.
36. Zeng, Z.; Yin, Z.; Huang, X.; Li, H.; He, Q.; Lu, G.; Boey, F.; Zhang, H. Single-Layer Semiconducting Nanosheets: High-Yield Preparation and Device Fabrication. *Angew. Chem., Int. Ed.* **2011**, *50*, 11093–11097.
37. Coleman, J. N.; Lotya, M.; O'Neill, A.; Bergin, S. D.; King, P. J.; Khan, U.; Young, K.; Gaucher, A.; De, S.; Smith, R. J.; *et al.* Two-Dimensional Nanosheets Produced by Liquid Exfoliation of Layered Materials. *Science* **2011**, *331*, 568–571.
38. Li, H.; Zhang, Q.; Yap, C. C. R.; Tay, B. K.; Edwin, T. H. T.; Olivier, A.; Baillargeat, D. From Bulk to Monolayer MoS_2: Evolution of Raman Scattering. *Adv. Funct. Mater.* **2012**, *22*, 1385–1390.
39. Zhu, C.; Zeng, Z.; Li, H.; Li, F.; Fan, C.; Zhang, H. Single-Layer MoS_2-Based Nanoprobes for Homogeneous Detection of Biomolecules. *J. Am. Chem. Soc.* **2013**, *135*, 5998–6001.
40. Chikan, V.; Kelley, D. F. Size-Dependent Spectroscopy of MoS_2 Nanoclusters. *J. Phys. Chem. B* **2002**, *106*, 3794–3804.
41. Wilcoxon, J. P.; Newcomer, P. P.; Samara, G. A. Synthesis and Optical Properties of MoS_2 and Isomorphous Nanoclusters in the Quantum Confinement Regime. *J. Appl. Phys.* **1997**, *81*, 7934–7944.
42. Wilcoxon, J. P.; Samara, G. A. Strong Quantum-Size Effects in a Layered Semiconductor: MoS_2 Nanoclusters. *Phys. Rev. B* **1995**, *51*, 7299–7302.
43. Enyashin, A. N.; Seifert, G. Density-Functional Study of Li_xMoS_2 Intercalates ($0 \leq x \leq 1$). *Comput. Theor. Chem.* **2012**, *999*, 13–20.
44. Sekine, T.; Julien, C.; Samaras, I.; Jouanne, M.; Balkanski, M. Vibrational Modifications on Lithium Intercalation in MoS_2. *Mater. Sci. Eng., B* **1989**, *3*, 153–158.
45. Chrissafis, K.; Zamani, M.; Kambas, K.; Stoemenos, J.; Economou, N. A.; Samaras, I.; Julien, C. Structural Studies of MoS_2 Intercalated by Lithium. *Mater. Sci. Eng., B* **1989**, *3*, 145–151.
46. Alexiev, V.; Prins, R.; Weber, T. *Ab Initio* Study of MoS_2 and Li Adsorbed on the (1010) Face of MoS_2. *Phys. Chem. Chem. Phys.* **2000**, *2*, 1815–1827.
47. Enyashin, A. N.; Yadgarov, L.; Houben, L.; Popov, I.; Weidenbach, M.; Tenne, R.; Bar-Sadan, M.; Seifert, G. New Route for Stabilization of 1T-WS_2 and MoS_2 Phases. *J. Phys. Chem. C* **2011**, *115*, 24586–24591.
48. Lukowski, M. A.; Daniel, A. S.; Meng, F.; Forticaux, A.; Li, L.; Jin, S. Enhanced Hydrogen Evolution Catalysis from Chemically Exfoliated Metallic MoS_2 Nanosheets. *J. Am. Chem. Soc.* **2013**, *135*, 10274–10277.
49. Papageorgopoulos, C. A.; Jaegermann, W. Li Intercalation Across and Along the van der Waals Surfaces of MoS_2 (0001). *Surf. Sci.* **1995**, *338*, 83–93.
50. Yun, J. M.; Noh, Y. J.; Yeo, J. S.; Go, Y. J.; Na, S. I.; Jeong, H. G.; Kim, J.; Lee, S.; Kim, S. S.; Koo, H. Y.; *et al.* Efficient Work-Function Engineering of Solution-Processed MoS_2 Thin-Films for Novel Hole and Electron Transport Layers Leading to High-Performance Polymer Solar Cells. *J. Mater. Chem. C* **2013**, *1*, 3777–3783.
51. Perdew, J. P.; Burke, K.; Ernzerhof, M. Generalized Gradient Approximation Made Simple. *Phys. Rev. Lett.* **1996**, *77*, 3865–3868.
52. Blochl, P. E. Projector Augmented-Wave Method. *Phys. Rev. B* **1994**, *50*, 17953–17979.
53. Kohn, W.; Meir, Y.; Makarov, D. E. van der Waals Energies in Density Functional Theory. *Phys. Rev. Lett.* **1998**, *80*, 4153–4156.
54. Grimme, S. Semiempirical GGA-Type Density Functional Constructed with a Long-Range Dispersion Correction. *J. Comput. Chem.* **2006**, *27*, 1787–1799.

55. Bhattacharyya, S.; Singh, A. K. Semiconductor-Metal Transition in Semiconducting Bilayer Sheets of Transition-Metal Dichalcogenides. *Phys. Rev. B* **2012**, *86*, 075454.
56. Boker, T.; Severin, R.; Muller, A.; Janowitz, C.; Manzke, R.; Voss, D.; Kruger, P.; Mazur, A.; Pollmann, J. Band Structure of MoS_2, $MoSe_2$, and α-$MoTe_2$: Angle-Resolved Photoelectron Spectroscopy and *Ab Initio* Calculations. *Phys. Rev. B* **2001**, *64*, 235305.